Aeolian Research 20 (2016) 147–156

Contents lists available at ScienceDirect

Aeolian Research

journal homepage: www.elsevier.com/locate/aeolia

Modeling of particulate matter transport in atmospheric boundary layer following dust emission from source areas

Itzhak Katra [a,*], Tov Elperin [b], Andrew Fominykh [b], Boris Krasovitov [b], Hezi Yizhaq [c,d]

[a] Department of Geography and Environmental Development, Ben-Gurion University of the Negev, P.O.B. 653, 84105, Israel
[b] Department of Mechanical Engineering, The Pearlstone Center for Aeronautical Engineering Studies, Ben-Gurion University of the Negev, P.O.B. 653, 84105, Israel
[c] Swiss Institute for Dryland Environmental and Energy Research, BIDR, Ben-Gurion University of the Negev, Midreshet Ben-Gurion, Israel
[d] The Dead Sea and Arava Science Center, Tamar Regional Council, Israel

ARTICLE INFO

Article history:
Received 2 May 2015
Revised 31 December 2015
Accepted 31 December 2015

Keywords:
Dust emission
Aeolian processes
Portable wind tunnel
Wind mast
PM_{10}
Advection–diffusion equation

ABSTRACT

A two-dimensional model for particulate matter (PM) dispersion due to dust emission from soils is presented. Field experiments were performed at a dust source site (Negev loess soil) with a portable boundary layer wind tunnel to determine the emitted PM fluxes for different wind speeds and varying soil conditions. The numerical model is formulated using parameterizations based on the aeolian experiments. The wind velocity profiles used in the simulations were fitted from data obtained in field measurements. Size distribution of the emitted dust particles in the numerical simulations was taken into account using a Monte Carlo method. The PM concentration distributions at a distance of several kilometers from the dust source under specific shear velocities and PM fluxes from the soil were determined numerically by solving advection–diffusion equation. The obtained PM_{10} concentrations under typical wind and soil conditions are supported by PM data recorded over time in a standard environmental monitoring station. The model enhances our capacity of quantification of dust processes to support climate models as well as health risk assessment.

1. Introduction

Mineral dust is a key agent involved in a wide range of physical, chemical and biological processes of the Earth system. Dust particles profoundly affect the energy, carbon and water cycles of the climate system (see e.g., Shao et al., 2011). It has been recognized that dust aerosol can also have significant impacts on human health. During dust storms, concentrations of dust particles having aerodynamic diameter less or equal to 10 μm (PM_{10}) in arid areas can exceed significantly the World Health Organization (WHO) guideline for air quality (Katra et al., 2014a), reaching outdoor and indoor concentrations in arid environments as high as 5000 and 1500 $\mu g/m^3$, respectively (Krasnov et al., 2015). Other studies highlighted the role of PM from natural dust as an important environmental pollutant for human health impacts (Vodonos et al., 2014; Yitshak-Sade et al., 2014).

Modeling of dust transport is of profound importance for understanding the dust cycle at different scales. It requires combined theoretical and experimental study of particle emission (in consequence of wind soil erosion) and dust transport in the atmospheric boundary layer (ABL). In particular, modeling of atmospheric dust dispersion requires reliable data on measured input variables, such as grain size distribution, wind speed, sediment properties, dust-emission rate (see, e.g., Gillies et al., 2006; Shao, 2008; Durán et al., 2011; Kok et al., 2012).

Understanding the role of dust in the Earth system has prompted intensive development of dust emission models since the late 1980s (Shao et al., 2011). These developments spurred the intensive efforts in the modeling of dust transport. Pilinis et al. (1987) developed a mathematical model that describes the evolution of size and chemical composition distribution of atmospheric aerosols based on a sectional representation of the size distribution, and treats dynamics and thermodynamics of multicomponent atmospheric aerosols. Lu and Shao (1999) developed a theoretical model for the prediction of dust emission rate caused by saltation bombardment, based on the dust volume removal caused by impacting sand grains as they plough into the soil surface. In the present study, the dust emission generated by saltation bombardment has been modeled from the perspective of volume removal by saltating particles as proposed by Lu and Shao (1999). As Lu and Shao (1999), Shao (2001) noted, more field measurements are required in order to verify this approach.

* Corresponding author. Tel.: +972 8 6428434; fax: +972 8 6472821.
E-mail address: katra@bgu.ac.il (I. Katra).

http://dx.doi.org/10.1016/j.aeolia.2015.12.004
1875-9637/

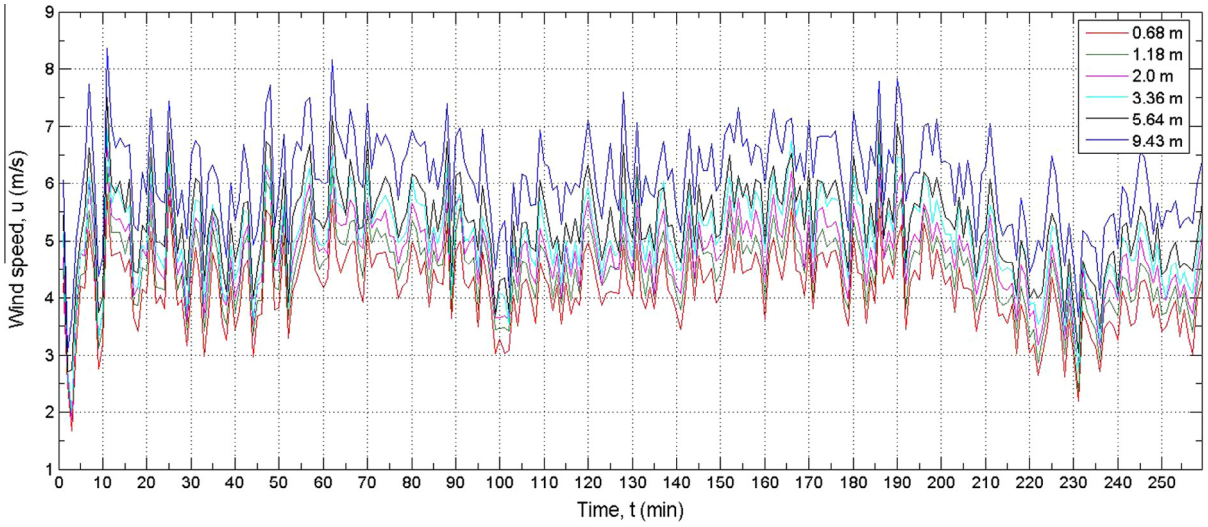

Fig. 1. Example of wind speed measured by the wind mast in the study area (June 12, 2014).

Table 1
Mean wind velocity vs. height based on field experiment of 12 June 2014.

Height, h (m)	Average wind velocity, $\bar{u}$ (m/s)
0.68	4.15
1.18	4.49
2.0	4.76
3.36	5.04
5.64	5.31
9.43	6.09

In spite of intensive development of advanced dust emission models, there is a gap in quantification of dust transport following dust emission from soils. Moreover, the knowledge about the impact of surface-property variability on dust fluxes from source areas is still severely lacking (Katra and Lancaster, 2008).

For individual wind-erosion events, wind shear near the surface is responsible for particle entrainment into the atmosphere, and turbulence in the atmospheric boundary layer is important for particle diffusion and deposition (Shao, 2008). Many of the early experiments on wind erosion (see e.g., Bagnold, 1936; Kawamura, 1951; Lettau, 1969; Lettau and Lettau, 1977; Nickling and Gillies, 1993; Bottema, 1996; MacDonald et al., 1998) show that in the case of negligible wake interference between the surface obstacles the mean velocity profile approaching each obstacle is logarithmic.

In this study, aeolian erosion under different wind and soil conditions in an area located in the northern Negev Desert (Israel) was simulated for modeling dust PM dispersion in the atmospheric boundary layer at a distance of several kilometers from the dust source. Field experiments were used to determine a set of parameters for the dust dispersion model that include dust emission fluxes and velocity profiles.

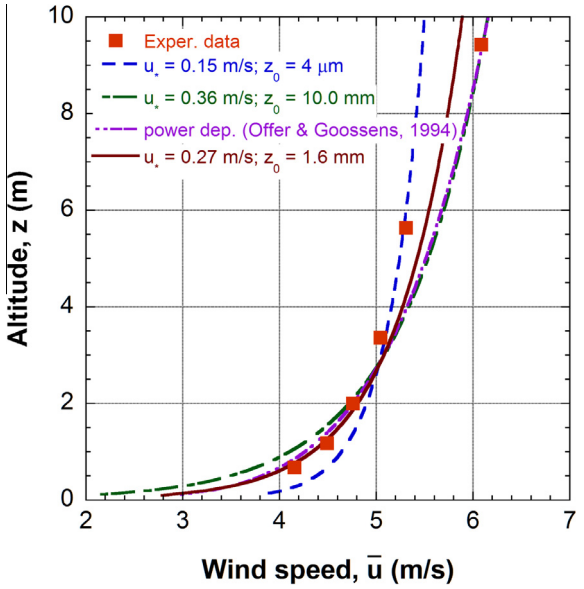

Fig. 2. Dependence of the average wind speed vs. altitude.

2. Mean wind velocity profile

The mean wind velocity profile for the studied case is required for simulating the PM dispersion after emission of dust from the soil. To this end we use standard equations of atmospheric boundary layer theory (see e.g., Shao, 2008). Goossens and Offer (1990) showed that in the Northern Negev area the depth of the Atmospheric Boundary Layer (ABL) is on the order of 500–600 m. Since we consider horizontal transport of dust particles over large distances, the assumptions of the validity of the boundary layer approximation are satisfied. Offer and Goossens (1994) showed that in the lowermost 15% of the ABL, the wind profile (in neutral atmospheric conditions) can be described either by the semi-empirical logarithmic law (see, e.g., Oke, 1987):

$$u = \frac{u_*}{\kappa} \ln\left(\frac{z}{z_0}\right) \tag{1}$$

or by the power law (see, e.g., Offer and Goossens, 1994):

$$u_1 = u_2 \left(\frac{z_1}{z_2}\right)^{\alpha}. \tag{2}$$

In Eq. (1) $u_* = \sqrt{\tau/\rho_a} \propto \sigma$ is friction velocity, which is a scaling parameter proportional to the velocity gradient in boundary layer flow; τ is the shear stress at the surface level and ρ_a is air density; σ is standard deviation of velocity fluctuations (see e.g., Bagnold, 1941; Shao, 2008; Kok et al., 2012); κ is the von Karman constant, $\kappa = 0.35 - 0.4$; z_0 is the aerodynamic surface roughness length

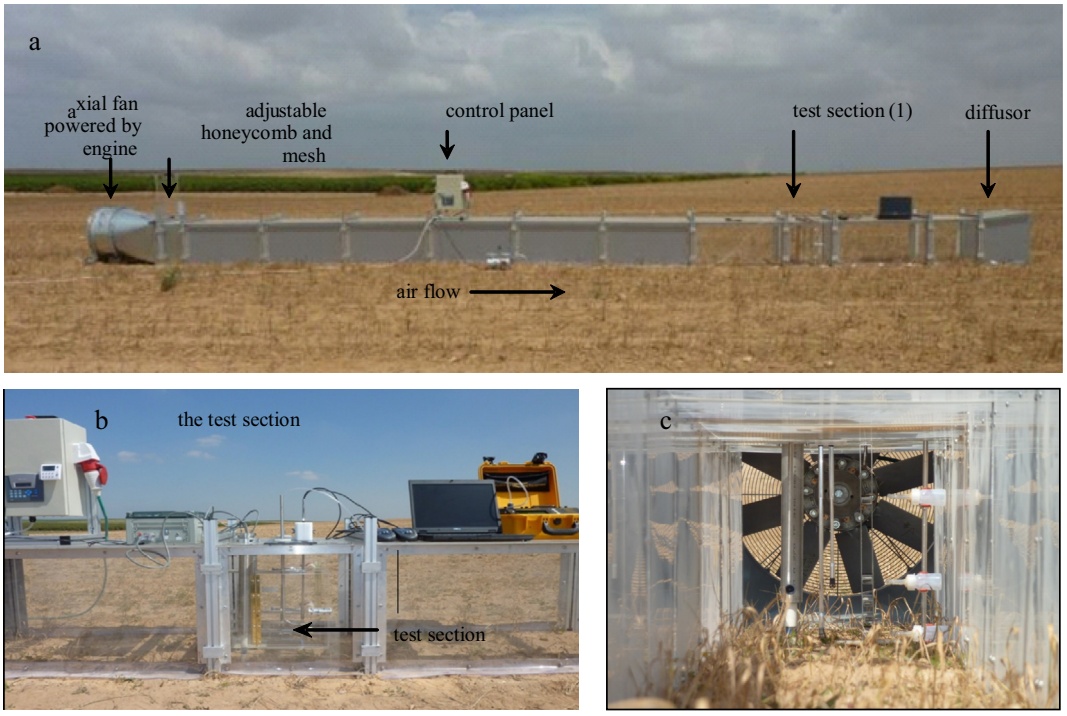

Fig. 3. The portable wind tunnel for field experiments on dust emission processes (Tanner et al., 2016). The tunnel segments are shown in the air-push configuration on a loess agricultural field (a). The cross sectional area is 0.5 × 0.5 m^2 and the test section length is up to 10 m (b). Instruments installed in the test section (c).

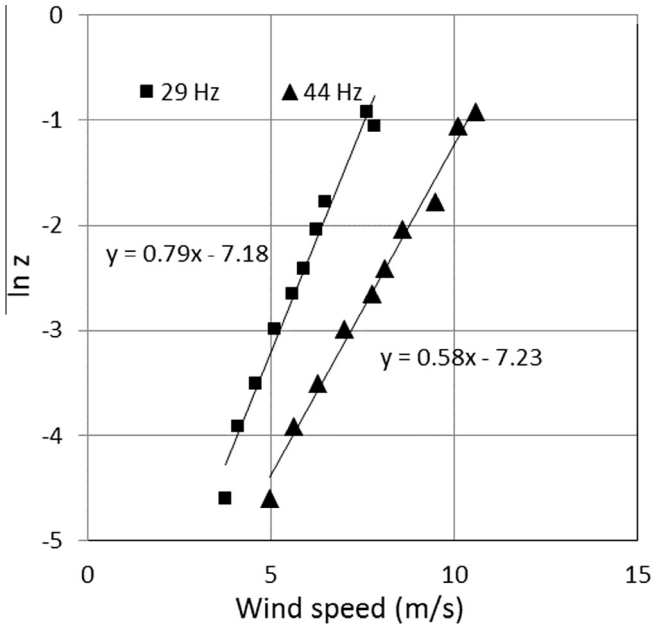

Fig. 4. Wind profiles measured in the portable wind tunnel in the loess bare soil (experimental plots) for fan frequencies of 29 Hz and 44 Hz.

that is approximately equal 1/30 of the field roughness elements height in turbulent flow. In the Negev area roughness elements' height (pebbles and shrubs) is of the order 0.2–0.3 m (Offer and Goossens, 1994). In Eq. (2) u_1 and u_2 are the mean wind speeds at heights z_1 and z_2, respectively. For the Negev area the value of the power law exponent α is in the range 0.16–0.17 (Offer and Goossens, 1994).

For this study, measurements of wind profiles were conducted in the Northern Negev with a wind mast in conjunction with experiments to quantify dust emission from the soils (see more details in the next section). A 10-meter wind mast was equipped with 6 cup anemometers positioned at: 0.68, 1.18, 2.0, 3.36, 5.64 and 9.43 m above ground level (AGL). The instruments record wind speeds in the range of 0–50 m/s with the accuracy of ±0.49 m/s and with a time interval of 1 min. The anemometers were calibrated in the laboratory before the field measurements. Wind speed measurements are shown in Fig. 1.

For each height the average wind speed was calculated as follows:

$$\bar{u} = \frac{1}{T - t_0} \int_{t_0}^{T} u(t)\, dt, \tag{3}$$

where t_0 is the initial time and $[t_0, T]$ is the time interval during which measurements were conducted. Average wind velocity at each height was determined by numerical integration of wind

Table 2
Results of particle fluxes from soils.

Area	Open area				Nature preserve			
Condition (soil)	Aggregated		Disaggregated		Aggregated		Disaggregated	
Frequency (Hz)	29	44	29	44	29	44	29	44
PM_{10} (mg m^{-2} min^{-1})	17.1	256.5	52.3	895.3	1.2	8.9	8.3	120.9

speed time series $u(t)$ using trapezoidal integration rule, and the obtained results are presented in Table 1.

The above dependence of the mean wind velocity vs. height was approximated by a logarithmic profile (see Eq. (1)) using the least squares method. Therewith the best fit to the observations is determined for the friction (shear) velocity $u_* = 0.27$ m/s and the roughness $z_0 = 1.6 \cdot 10^{-3}$ m with 95% confidence bounds. The results of calculations of the mean wind velocity as function of altitude are showed in Fig. 2.

In Fig. 2 the mean wind speed profiles were calculated using two different values of roughness, $z_0 = 4.0\ \mu$m and $z_0 = 10.0$ mm. Roughness $z_0 = 4.0\ \mu$m is calculated as 1/30 of the roughness elements corresponding to the large particles with the size of 120 μm (Bagnold, 1941), while the roughness $z_0 = 10.0$ mm corresponds to the roughness elements such as rocks and shrubs at the Negev area (see Offer and Goossens, 1994). The values of shear velocity for these aerodynamic roughness values are $u_* = 0.15$ m/s and $u_* = 0.36$ m/s, respectively. The double dot-dashed line in Fig. 2 describes the power law (3) where $u_2 = 4.76$ m/s is the magnitude of the mean wind velocity at the height $z_2 = 2$ m (see Table 1).

3. Aeolian experiments on dust emission

Boundary-layer wind tunnels enable aeolian simulations under standardized quasi-natural wind conditions (Leys and Raupach, 1991; Shao, 2008) and provide quantitative information on aeolian particle transport including sand fluxes (Katra et al., 2014b) and dust emission rates from soils (Houser and Nickling, 2001; Sharratt et al., 2010; Singh et al., 2012; Van Pelt et al., 2013). The wind-tunnel experiments were conducted in the loess soil of the northern Negev. Many of the loess soils throughout the world are associated with wind erosion activity, which is largely a result of environmental changes such as droughts and increased human activities, thereby amplifying dust emissions from the disturbed surfaces. These soils contain a significant fraction of silt and clay (<50 μm), 71.6% in nature preserve and 64.2% in open area. The presence of a sand fraction in its loamy texture enables the entrainment of fine particles by ballistic impact (saltation bombardment) (Kok et al., 2012). The measurements were conducted in experimental plots of bare and dry soils representing common surfaces in the Northern Negev: open area – an area with human activities that is mainly grazing, and a nature preserve – where human activities are highly restricted. In both cases the soils were tested in two different conditions of the topsoil: undisturbed (aggregated), and disturbed (disaggregated) conditions. In the latter condition, the soils were treated in the field to simulate a short-term disturbance of human activities by mechanical operation (Bacon et al., 2011) for a reduced soil aggregation. The portable boundary-layer wind tunnel has been designed to study dust emission in the field by simulating aeolian processes (Fig. 3). The wind tunnel has a cross sectional area of 0.5×0.5 m^2, with an open-floored working section up to 10 m long. Air push or air suction flow in the tunnel is generated by an axial fan up to maximum speed of 18 m s^{-1} measured along the centerline. Instruments installed in the test section of the tunnel enable quantification of: (1) the vertical wind speed profile for calculating friction velocity and aerodynamic roughness height, (2) saltation flux, and (3) dust concentration profile including PM_{10}.

The wind tunnel was operated at the experimental plots at fan frequencies (wind speeds) of 23 Hz (4 ms^{-1}) and 44 Hz (9 ms^{-1}), which represent the minimum wind speed required for aeolian erosion and an average wind speed in dust storms in the study area, respectively. For each fan frequency the wind speed was measured during testing for the specific soils. The measured vertical velocity profiles in the wind tunnel (see Fig. 4) exhibit the same semi-log form as velocity profiles determined in the experiments with a wind mast (see Table 1 and Fig. 2).

At the beginning of each test, the concentration of the suspended particles in the wind tunnel was measured by a real-time dust monitor for background PM_{10} values (DustTrak 8534, TSI). The DustTrak installed in the test section (Fig. 3) recorded PM concentration (μg m^{-3}) at 1 Hz.

Each experiment (surface/condition/frequency) was performed in three replicates with a run time of 600 s. The recorded PM_{10} data (concentration) was converted into mass flux emitted from the soil surface (F_{PM}) based on the wind tunnel dimensions and area of the experimental plot:

$$F_{PM} = C_{PM} V_t / (A_p t) \tag{4}$$

where C_{PM} is the recorded PM concentrations (mg m^{-3}), V_t is the volume air in the wind tunnel (1.85 m^3), A_p is the area of the experimental plot (3.75 m^2), and t is time (in minutes).

The obtained results (see Table 2) demonstrate the dependence of dust emission in surface variability and wind speed. Overall, there were higher dust fluxes from the open area as compared to the natural preserve. The open area is subjected to grazing activities, which impact the topsoil properties and reduce the surface stability against erosion. Analyses of the topsoil properties show lower contents of soil cementing material (e.g., soil organic matter, clays, calcium carbonate) in the open area compared to the natural preserve and therefore lower content of large aggregates. Such differences in the soil properties between grazing and natural plots have been demonstrated in previous studies (see e.g., Singh et al., 2012; Tanner et al., 2016). It is generally assumed that soils with a greater amount of large aggregates have stronger resistance against erosion. Only a few studies referred to the soil aggregation in aeolian processes, but with a focus on the wind erodible fraction (EF) (aggregates in diameter of <840 μm) (Zobeck et al., 2013). In both experimental plots, higher wind speed (corresponding to larger fan frequency) and disturbed topsoil (disaggregation) increase the PM_{10} fluxes from the soil. These results were used for parameterization of dust fluxes in the numerical simulations.

4. Numerical simulations

Atmospheric dust concentration at given time and location can be described by the advection–diffusion equation for dust particles (see e.g., Shao et al., 2011):

$$\frac{\partial c}{\partial t} + u\frac{\partial c}{\partial x} + v\frac{\partial c}{\partial y} + (w - w_t)\frac{\partial c}{\partial z} = \frac{\partial}{\partial x}\left(K_{px}\frac{\partial c}{\partial x}\right) + \frac{\partial}{\partial y}\left(K_{py}\frac{\partial c}{\partial y}\right) + \frac{\partial}{\partial z}\left(K_{pz}\frac{\partial c}{\partial z}\right) + S_r + S_c \tag{5}$$

where u, v and w are the velocities in x, y and z directions; K_{px}, K_{py} and K_{pz} are the dust-particle eddy diffusivities for the x, y and z directions, w_t is dust particle sedimentation velocity, S_r is a source (or sink) term arising from wet removal and S_c is a source (or sink) term arising from the dust-flux convergence due to dry and wet convections.

In our model, we consider only dust transport in the layer close to the surface where atmospheric parameters (e.g., wind speed, temperature, aerosol concentration) vary rapidly with height, and turbulence is predominantly generated by wind shear. In this layer the effects of stratification are secondary. Consequently, it is assumed that vertical motion of air is inhibited and particles are transported by advection in horizontal direction. Hereafter we assume that the wind is unidirectional and the wind velocity

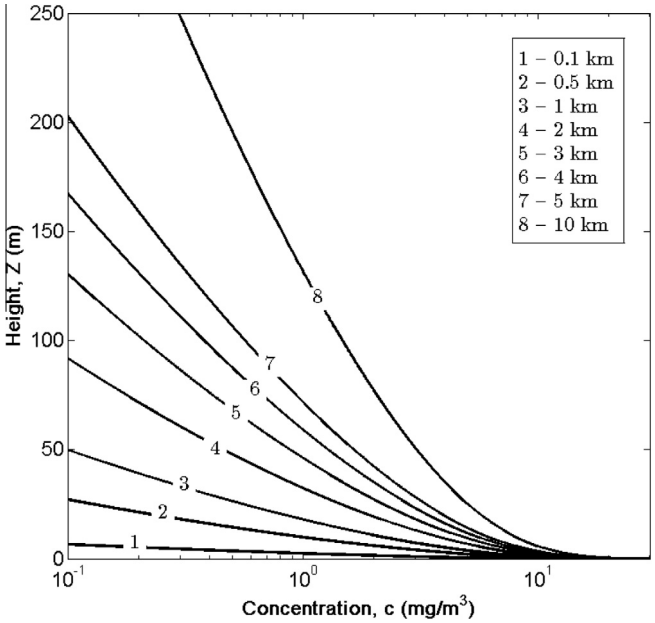

Fig. 5. Dust (PM_{10}) concentration profiles at the different distances from the origin of the source area. (length of the source area $x_S = 10$ km).

depends on the vertical coordinate only (see Eq. (1)). In the steady-state case the Eq. (5) can be rewritten as follows:

$$u\frac{\partial c}{\partial x} - w_t\frac{\partial c}{\partial z} = \frac{\partial}{\partial z}\left(K_{pz}\frac{\partial c}{\partial z}\right). \tag{6}$$

The boundary conditions for Eq. (6) read:

$$w_t c - K_{pz}\frac{\partial c}{\partial z} = Q_0[1 - H(x - x_S)] \quad at \quad z = 0 \tag{7}$$

$$K_{pz}\frac{\partial c}{\partial z} = 0 \quad at \quad z = h \tag{8}$$

$$c(0, z) = 0, \tag{9}$$

where h is the height of the ABL. In the calculations we assumed that $h = 500$ m.

In Eqs. (6)–(9) Q_0 is the net dust flux at the surface, $H(x)$ is Heaviside step function, x_S is the length of the source area and w_t is the terminal settling velocity of deposited dust particles (Seinfeld and Pandis, 2006, p. 408):

$$w_t = \frac{1}{18}\frac{d_p^2 \rho_p g C_c}{\mu}, \tag{10}$$

where d_p is the diameter of the dust particle, ρ_p is the density of the dust particle; g is gravitational acceleration; C_c is the Cunningham slip correction factor; μ is the coefficient of the dynamic viscosity of the air. Estimations show that for dust particles with the diameter $d_p = 10\,\mu$m and density $\rho_p = 2.6$ g/cm^3 the terminal settling in air velocity is $\approx 7.9 \cdot 10^{-3}$ m/s. For a dust particle with the diameter $d_p = 120\mu$m the terminal velocity is on the order of 1 m/s.

The coefficient of eddy diffusivity can be calculated as follows (see e.g., Shao, 2008):

$$K_{pz} = \kappa u_* z. \tag{11}$$

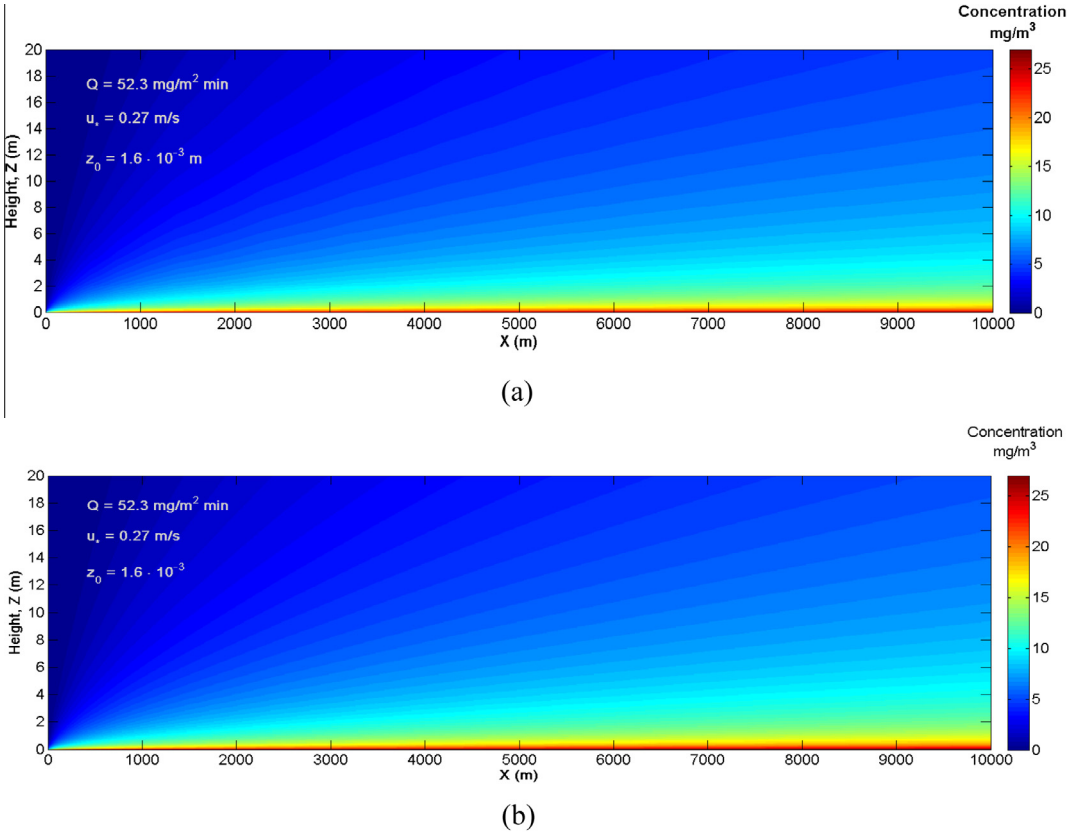

Fig. 6. Distribution of dust particles concentration calculated in XZ-plane at $Y = 0$ (friction velocity $u_* = 0.27$ m/s, aerodynamic roughness $z_0 = 1.6 \cdot 10^{-3}$ m, dust flux at the surface $Q_0 = 52.3$ mg m^{-2} min^{-1} – non-cohesive state): (a) diameter of the particles $d_p = 10\,\mu$m; (b) log-normal distribution of particles diameter is taken into account ($d_r = 10\,\mu$m, $d_r/\sigma_r = 0.3$).

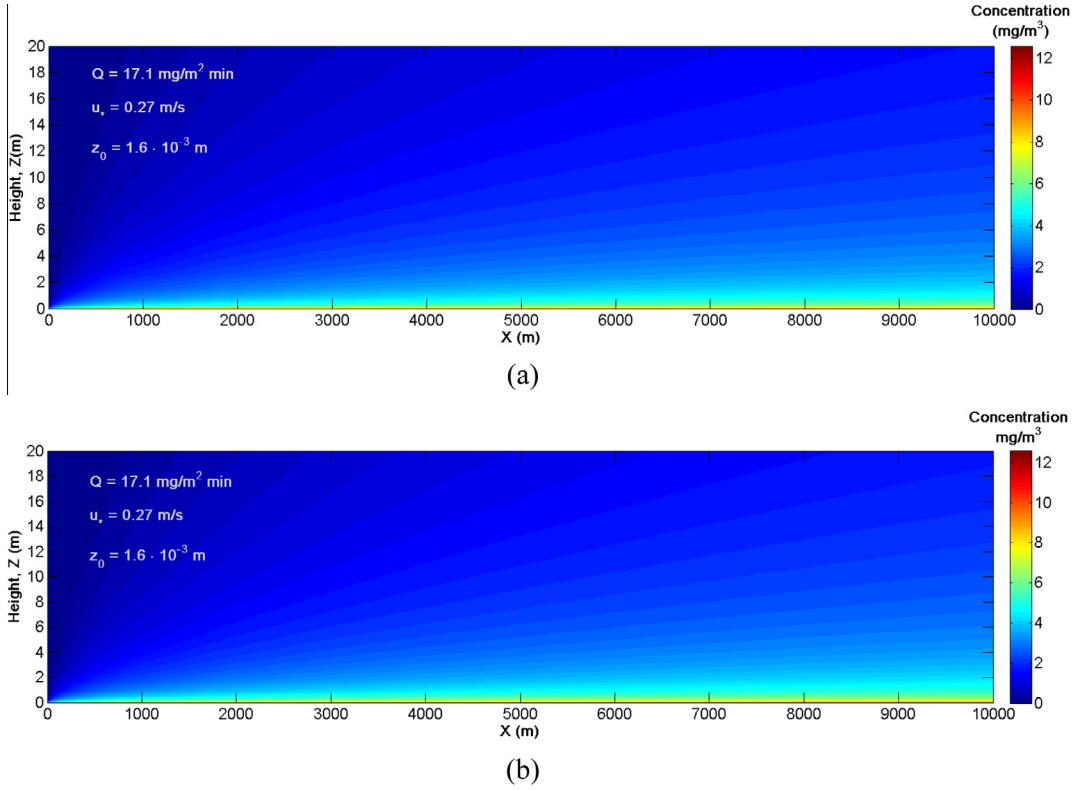

Fig. 7. Distribution of dust particles concentration calculated in *XZ*-plane at $Y = 0$ (friction velocity $u_* = 0.27$ m/s, aerodynamic roughness $z_0 = 1.6 \cdot 10^{-3}$ m, dust flux at the surface $Q_0 = 17.1$ mg m^{-2} min^{-1} – non-cohesive state): (a) diameter of the particles $d_p = 10$ μm; (b) log-normal distribution of particle diameter is taken into account ($d_r = 10$ μm, $\sigma_r/d_r = 0.3$).

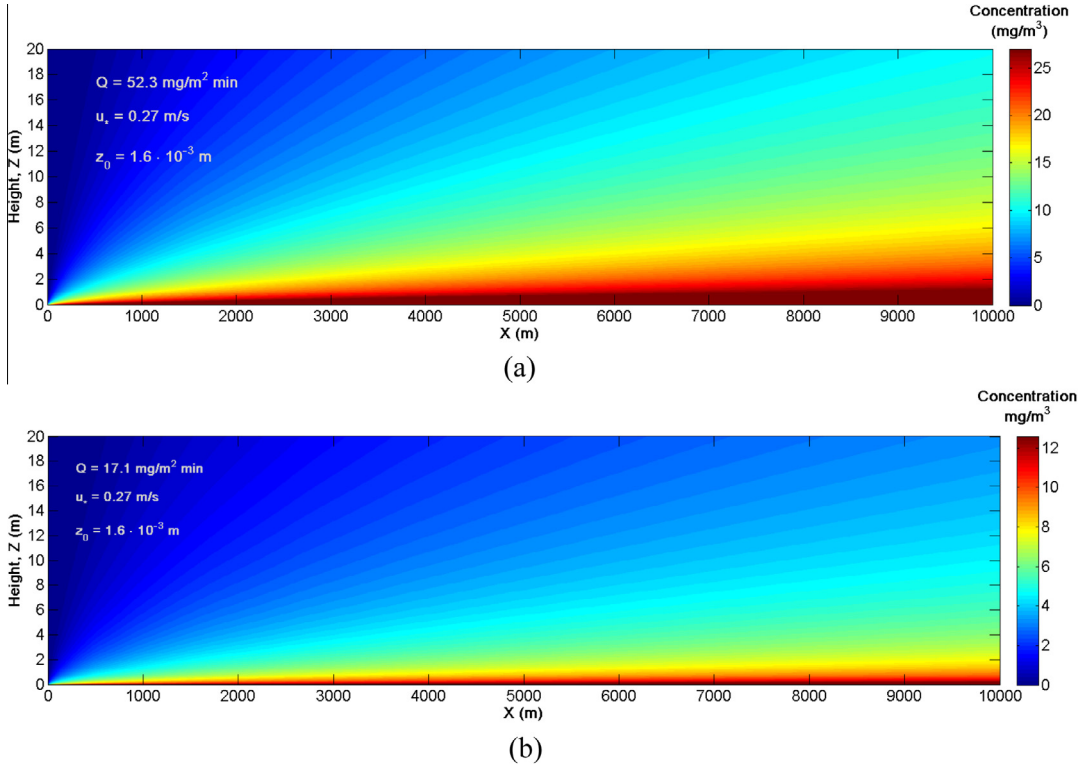

Fig. 8. Distribution of dust particles concentration calculated in *XZ*-plane at $Y = 0$ (friction velocity $u_* = 0.27$ m/s, aerodynamic roughness $z_0 = 1.6 \cdot 10^{-3}$ m, log-normal distribution of particle diameter is taken into account –$d_r = 5$ μm, $\sigma_r/d_r = 0.3$); (a) dust flux at the surface $Q_0 = 52.3$ mg m^{-2} min^{-1} (non-cohesive state); (b) dust flux at the surface $Q_0 = 17.1$ mg m^{-2} min^{-1} (cohesive state).

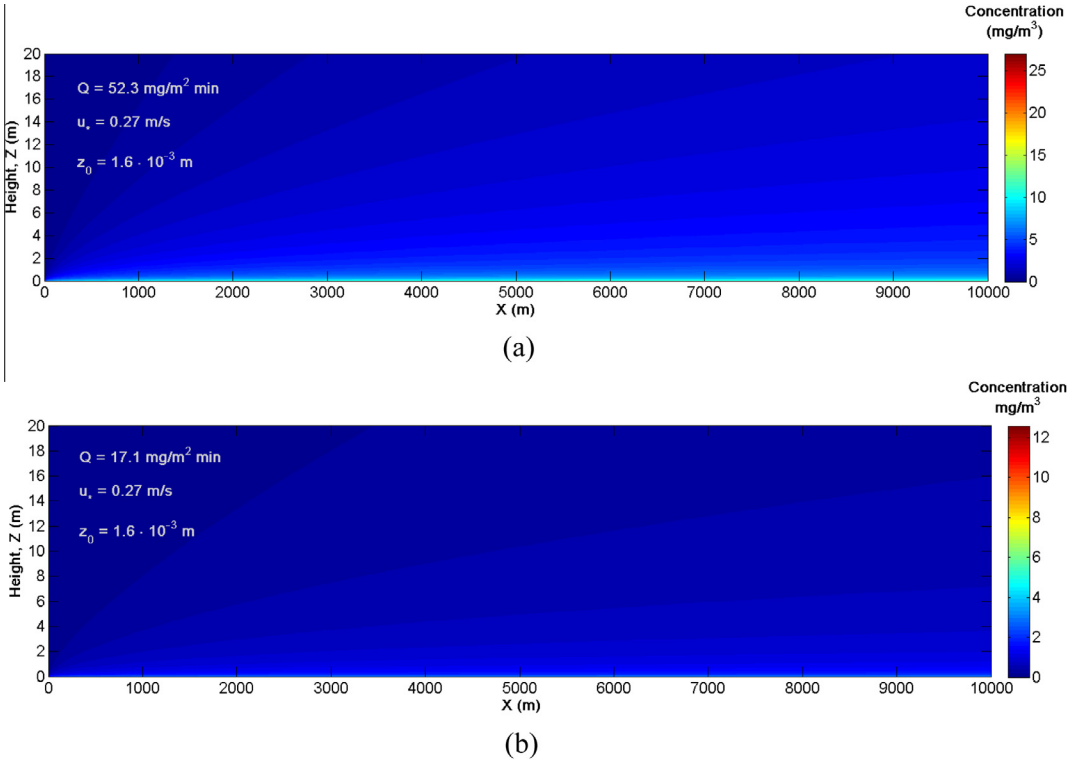

Fig. 9. Distribution of dust particles concentration calculated in *XZ*-plane at $Y = 0$ (friction velocity $u_* = 0.27$ m/s, aerodynamic roughness $z_0 = 1.6 \cdot 10^{-3}$ m, log-normal distribution of particle diameter is taken into account –$d_r = 20$ μm, $d_r/\sigma_r = 0.3$); (a) dust flux at the surface $Q_0 = 52.3$ mg m^{-2} min^{-1} (non-cohesive state); (b) dust flux at the surface $Q_0 = 17.1$ mg m^{-2} min^{-1} (cohesive state).

Transport of dust particles by turbulent diffusion as well as dust particles deposition strongly depends on the dust particle diameter. In our calculations we assumed a log-normal size distribution for the dust particles:

$$f(d_p) = \frac{1}{\sqrt{2\pi}\sigma d_p} e^{-\frac{(\ln d_p - \mu)^2}{2\sigma^2}} \tag{12}$$

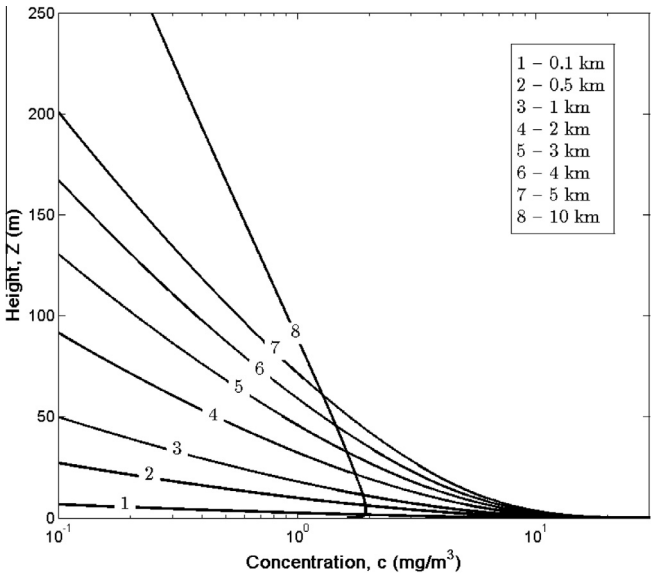

Fig. 10. Dust (PM_{10}) concentration profiles at different distances from the origin of the source area vs. height (length of the source area $x_S = 5$ km).

Parameters μ and σ of the log-normal distribution are determined by d_r and σ_r, mean and variance of particle size distribution, respectfully:

$$\sigma = \sqrt{\ln\left(\frac{\sigma_r^2}{d_r^2} + 1\right)}, \quad \mu = \ln d_r - \frac{\sigma^2}{2}.$$

These parameters can be estimated as follows:

$$d_r = \frac{1}{N}\sum_{i=1}^{N} d_{p,i}, \quad \sigma_r^2 = \frac{1}{N-1}\sum_{i=1}^{N}(d_{p,i} - d_r)^2,$$

where $d_{p,i}$ are measured diameters of dust particles and N is the number of measurements.

Numerical analysis of a dust transport model described by the advection–diffusion equation (6) supplemented with the initial and boundary conditions (7)–(9) was performed using MATLAB numerical toolbox. Particle size distribution was taken into account using the Monte Carlo method whereby the particle concentration distribution was calculated by solving the initial boundary-value problem given by Eq. (6) for a particle diameter that was randomly sampled from the probability density function (12). The particle concentration distribution was determined by averaging over an ensemble of 1000 particle concentration distributions determined for randomly chosen particle diameters. The Monte Carlo algorithm was implemented into a MATLAB routine and integrated into the dust transport model.

5. Results and discussion

The model was applied to the calculations of dust emission and transport from different area sources with lengths 3, 5 and 10 km. Calculations were performed for particles with average

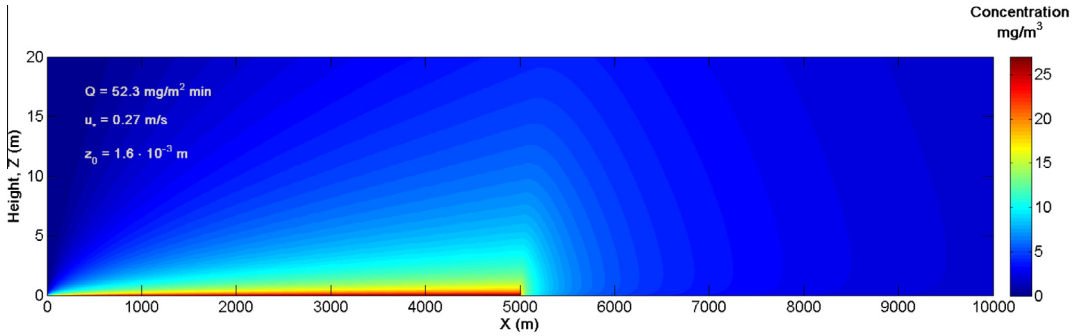

Fig. 11. Distribution of dust particles PM_{10} concentration calculated in *XZ*-plane at $Y = 0$ (shear velocity $u_* = 0.27$ m/s, the roughness $z_0 = 1.6 \cdot 10^{-3}$ m, log-normal distribution of particle diameter, source area length $x_S = 5$ km).

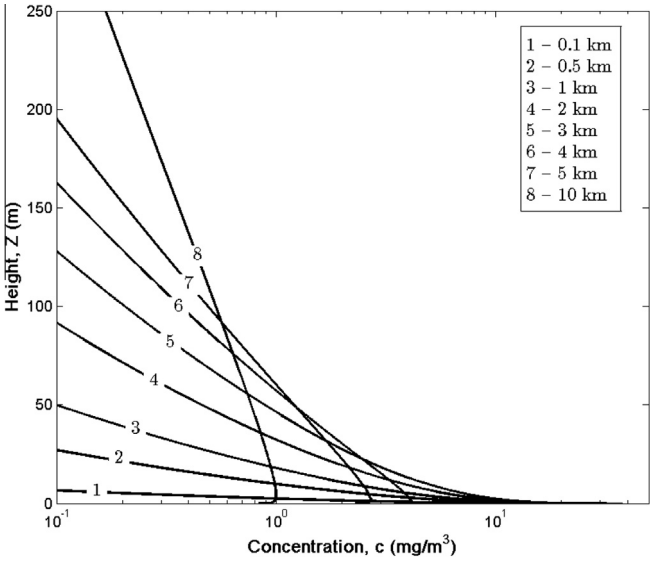

Fig. 12. Dust (PM_{10}) concentration profiles at the different distances from the origin of the source area vs. height (length of the source area $x_S = 3$ km).

aerodynamic diameters 5, 10 and 20 μm as well as for PM_5, PM_{10} and PM_{20}. In numerical simulations we used Monte-Carlo method whereby the advection–diffusion equation was solved for 1000 particle diameters sampled from the log-normal distribution given by Eq. (12). The particle concentration distribution was determined as average of these solutions. It was assumed that the wind velocity profile is determined by Eq. (1) where the friction velocity and aerodynamic roughness are determined by fitting the experimental data ($u_* = 0.27$ m/s and $z_0 = 1.61 \cdot 10^{-3}$ m) and the measured dust fluxes $Q_0 = 52.3$ mg m^{-2} min^{-1} and $Q_0 = 17.1$ mg m^{-2} min^{-1} in open area for the aggregated and disaggregated conditions, respectively (see Table 2).

Results of calculation of dust (PM_{10}) concentration profiles are shown in Fig. 5. In this case the length of the source area was assumed to be 10 km. Calculations were performed for dust flux $Q_0 = 52.3$ mg m^{-2} min^{-1}, and different distances from the origin of the source area, namely 0.1, 0.5, 1, 2, 3, 4, 5 and 10 km. Inspection of the obtained vertical concentration profiles shows that the maximum concentration of PM_{10} at the ground exceeds 35 mg m$-^3$.

Results of calculations of the concentration distribution of the dust particles ($d_p = 10$ μm) near the ground for two values of dust flux $Q_0 = 52.3$ mg m^{-2} min^{-1} and $Q_0 = 17.1$mg m^{-2} min^{-1} are shown in Figs. 6 and 7, respectively.

Calculations for monosize particles with the diameter 10 μm and dust fluxes $Q_0 = 52.3$ mg m^{-2} min^{-1} and $Q_0 = 17.1$ mg m^{-2} min^{-1} are presented in Figs. 6a and 7a. Figs. 6b and 7b present the results of calculations taking into account the log-normal distribution of particle diameter (in this case $d_r = 10$ μm, $\sigma_r/d_r = 0.3$) and for dust fluxes $Q_0 = 52.3$ mg m^{-2} min^{-1} and $Q_0 = 17.1$ mg m^{-2} min^{-1}, respectively.

Dust particle concentrations decrease with height and increase in *x*-direction at low height level (near the ground) along the linear dust source (see Figs. 6 and 7). Comparison of the results of calculations (see Fig. 6a and b and Fig. 7a and b) shows that neglecting of particle size distribution may result in underestimation of particles concentrations in vertical direction.

Results of calculations of the concentration distribution of the dust particles taking into account particles size distributions for different values of the mean are shown in Figs. 8 and 9. Calculations were performed for the two values of dust flux $Q_0 = 52.3$ mg m^{-2} min^{-1} and $Q_0 = 17.1$ mg m^{-2} min^{-1}. Parameters d_r and σ_r of log-normal distribution (see Eq. (12)) were assumed

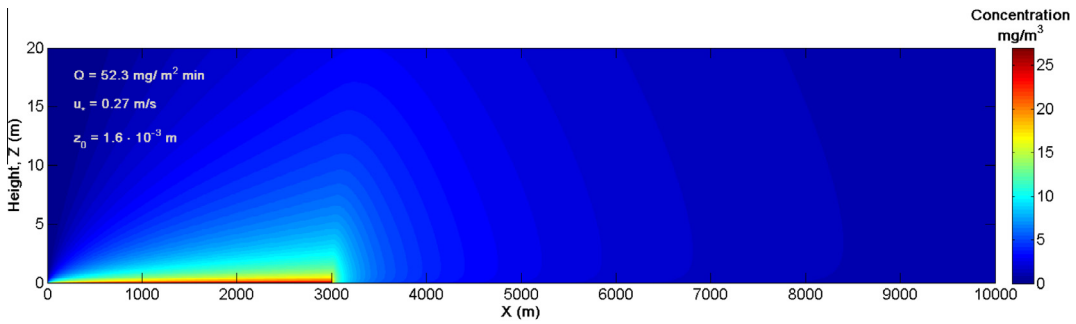

Fig. 13. Distribution of dust particles PM_{10} concentration calculated in *XZ*-plane at $Y = 0$ (shear velocity $u_* = 0.27$ m/s, aerodynamic roughness $z_0 = 1.6 \cdot 10^{-3}$ m, log-normal distribution of particle diameter, source area length $x_S = 3$ km).

to be 5 μm and 20 μm and $\sigma_r = 0.3\,d_r$, correspondingly. The results revealed that the concentration of the dust particles strongly depends on the size of the particles.

Results of calculations of dust (PM_{10}) concentration profiles for a source area $x_S = 5$ km are shown in Fig. 10. The dust flux was assumed to be $Q_0 = 52.3$ mg m^{-2} min^{-1}, and we used a logarithmic wind velocity profile corresponding to friction velocity $u_* = 0.27$ m/s and aerodynamic roughness $z_0 = 1.6 \cdot 10^{-3}$ m.

Results of calculations of the concentration distribution of PM_{10} near the ground emitted from source area with the length 5 km are shown in Fig. 11. Note that particles are advected beyond the length of the source area, and PM concentration distribution sharply changes outside the source area.

We also performed calculation of dust (PM_{10}) concentration profiles and concentration distribution of PM_{10} near the ground emitted from source area with length of $x_S = 3$ km. The results are shown in Figs. 12 and 13, correspondingly.

The study clearly demonstrates the impact of surface-property variability on dust fluxes (Table 2) and thus on the results of dust and PM transport models. The performed numerical calculations (see Figs. 5–13) show that at the distance of several kilometers from the dust source there are high atmospheric particulate matter (PM) concentrations in terms of air quality. According to the WHO guidelines the low end of the range of concentrations at which adverse health effects has been demonstrated is not greatly above the background concentration, which for particles smaller than 10 μm (PM_{10}) has been estimated to be 0.050 mg m$-^3$. Note that the high concentrations due to dust emission from this source area (bare and dry loess soil in a semi-arid zone) occurs even under the conditions of relatively low friction velocity (0.27 m/s) and undisturbed soils (dust flux at the surface $Q_0 = 17.1$ mg m^{-2} min^{-1}). At 10 m height, the results show about 2.5 mg m^{-3} and 4.5 mg m^{-3} for PM_{10} and PM_5, respectively (Figs. 6b and 7b). The simulation results of PM_{10} concentrations were compared with the recorded data in a monitoring station located at a distance of about 10 km west from the dust source (open area, Table 2). The monitoring station records PM_{10} data at height of 10 m by a dichotomous ambient particulate monitor (Thermo Scientific 1405DF; Thermo Fisher Scientific Inc.), which provides a continuous direct measurement of particle mass utilizing two tapered element oscillating microbalances (TEOMs). PM_{10} analysis for the period of 2001–2012 enabled detection of dust storms in the study area (Krasnov et al., 2014). Krasnov et al. (2014) demonstrated that during dust storms PM_{10} concentration can reach as much as 6 mg m^{-3} in the studied area when westerly winds are involved in the synoptic systems. Although dust arriving at the monitoring station does not originate only from the open area used for the experiments in this study, the simulation results provide a realistic prediction of PM spatial distribution in such arid environments.

6. Conclusions

We present a model for particulate matter distribution due to dust emission from a soil source in North Negev Desert region. Empirical parameters are derived from field measurements of wind profiles and experiments on emitted dust fluxes under different wind speeds and varying soil conditions. The experiments allowed us to take into account variations in dust emission from the source area (loess soil), and to reveal variations in the two-dimensional PM dispersion at distances of several kilometers from the origin of dust sources. Size distribution of the emitted dust particles in the numerical simulations was taken into account using a Monte Carlo method whereby the solution of the advection–diffusion equation for dust particles was averaged over the ensemble of 1000 solutions. Notably, numerical simulations to estimate atmospheric PM concentrations that used parameterizations based on measurements closely match atmospheric PM observed during dust storms. These findings demonstrate that using parametrization based on direct field measurements of wind profile and aeolian erosion has a potential to reduce uncertainties in atmospheric PM distribution models and provide more realistic assessment of dust concentration distribution. Moreover, such models can improve our understanding on loss of soil resources such as in agricultural fields due to wind erosion as well as on air pollution and exposure risks in urban environments located close to dust sources.

Acknowledgments

This research was partially supported by the Israel Science Foundation governed by the Israeli Academy of Sciences (Grants 1037/11, 1100/11 and 1210/15).

References

Bacon, S.N., McDonald, E.V., Amit, R., Enzel, Y., Crouvi, O., 2011. Total suspended particulate matter emissions at high friction velocities from desert landforms. J. Geophys. Res.: Earth Surf. 116 (F3).

Bagnold, R.A., 1936. The movement of desert sand. Proc. R. Soc. London. Ser. A Math. Phys. Sci. 157 (892), 594–620.

Bagnold, R.A., 1941. The Physics of Blown Sand and Desert Dunes. Methuen, New York.

Bottema, M., 1996. Roughness parameters over regular rough surfaces: experimental requirements and model validation. J. Wind Eng. Ind. Aerodyn. 64 (2–3), 249–265.

Durán, O., Claudin, P., Andreotti, B., 2011. On aeolian transport: grain-scale interactions, dynamical mechanisms and scaling laws. Aeolian Res. 3, 243–270. http://dx.doi.org/10.1016/j.aeolia.2011.07.006.

Gillies, J.A., Nickling, W.G., King, J., 2006. Aeolian sediment transport through large patches of roughness in the atmospheric inertial sublayer. J. Geophys. Res. Earth Surf. 111. http://dx.doi.org/10.1029/2005JF000434.

Goossens, D., Offer, Z., 1990. A wind tunnel simulation and field verification of desert dust deposition (Avdat Experimental Station, Negev Desert). Sedimentology 37, 7–22.

Houser, C.A. and Nickling, W.G., 2001. The emission and vertical flux of particulate matter <10 μm from a disturbed clay-crusted surface, Sedimentology 48, 255–267.

Katra, I., Lancaster, N., 2008. Surface-sediment dynamics in a dust source from spaceborne multispectral thermal infrared data. Remote Sens. Environ. 12 (7), 3212–3221. http://dx.doi.org/10.1016/j.rse.2008.03.016.

Katra, I., Arotsker, L., Krasnov, H., Zaritski, A., Kushmaro, A., Ben-Dov, A., 2014a. Richness and diversity in dust stormborne biomes at the Southeast Mediterranean. Sci. Rep. 4, 5265. http://dx.doi.org/10.1038/srep05265.

Katra, I., Yizhaq, H., Kok, J.F., 2014b. Mechanisms limiting the growth of Aeolian Megaripples. Geophys. Res. Lett. 41, 858–865.

Kawamura, R., 1951. Study of sand movement by wind. Rep. Phys. Sci. Res. Inst. 5(3–4), University of Tokyo, 95–112.

Kok, J.F., Parteli, E.J.R., Michaels, T.I., Bou Karam, D., 2012. The physics of windblown sand and dust. Rep. Prog. Phys. 75, 106901. http://dx.doi.org/10.1088/0034-4885/75/10/106901.

Krasnov, H., Katra, I., Koutrakis, P., Friger, M., 2014. Contribution of dust storms to PM_{10} levels in an urban arid environment. J. Air Waste Manage. Assoc. 64, 89–94.

Krasnov, H., Katra, I., Novack, V., Vodonos, A., Friger, M., 2015. Increased indoor PM concentrations controlled by atmospheric dust events and urban factors. Build. Environ. 87, 169–176. http://dx.doi.org/10.1016/j.buildenv.2015.01.035.

Lettau, H., 1969. Note on aerodynamic roughness-parameter estimation on the basis of roughness-element description. J. Appl. Meteorol. 8, 828–832.

Lettau, K., Lettau, H., 1977. Experimental and micrometeorological field studies of dune migration. In: Lettau, K., Lettau, H. (Eds.), Exploring the World's Driest Climate. Center for Climatic Research, University of Wisconsin-Madison, IES Report, 101, pp. 110–147.

Leys, J.F., Raupach, M.R., 1991. Soil flux measurements using a portable wind erosion tunnel. Aust. J. Soil Res. 29, 533–552.

Lu, H., Shao, Y., 1999. A new model for dust emission by saltation bombardment. J. Geophys. Res. 104, 16827–16842.

MacDonald, R.W., Griffiths, R.F., Hall, D.J., 1998. An improved method for the estimation of surface roughness of obstacle arrays. Atmos. Environ. 32 (11), 1857–1864.

Nickling, W.G., Gillies, J.A., 1993. Dust emission and transport in Mali, West Africa. Sedimentology 40, 859–868.

Offer, Z.Y., Goossens, D., 1994. The use of topographic scale models in predicting eolian dust erosion in hilly areas: field verification of a wind tunnel experiment. Catena 22, 249–263.

Oke, T.R., 1987. Boundary Layer Climates, second ed., Methuen, pp. 435.

Pilinis, C., Seinfeld, J.H., Seigneur, C., 1987. Mathematical modeling of the dynamics of multicomponent atmospheric aerosols. Atmos. Environ. 21, 943–955.
Seinfeld, J.H., Pandis, S.N., 2006. Atmospheric Chemistry and Physics. From Air Pollution to Climate Change. John Wiley & Sons, New York.
Shao, Y., 2001. A model for mineral dust emission. J. Geophys. Res. 106 (D17), 20239–20254.
Shao, Y., 2008. Physics and Modelling of Wind Erosion. Kluwer Academic Publishers, Dordrecht.
Shao, Y., Wyrwoll, K.-H., Chappell, A., Huang, J., Lin, Zhaohui, McTainsh, G.H., Mikami, M., Tanaka, T.Y., Wang, X., Yoon, S., 2011. Dust cycle: an emerging core theme in Earth system science. Aeolian Res. 2, 181–204.
Sharratt, B., Wendling, L., Feng, G., 2010. Windblown dust affected by tillage intensity during summer fallow. Aeolian Res. 2, 129–134.
Singh, P., Sharratt, B., Schillinger, W.F., 2012. Wind erosion PM10 emission affected by tillage system in the world's driest rainfed wheat region. Soil Till. Res. 124, 219–225.
Tanner, S., Katra, I., Haim, A., Zaady, E., 2016. Short-term soil loss by aeolian erosion in response to conventional and organic agricultural practices. Soil Till. Res. 155, 149–156.
Van Pelt, R.S., Baddock, M.C., Zobeck, T.M., Schlegel, A.J., Vigil, M.F., Acosta Martinez, V., 2013. Field wind tunnel testing of two silt loam soils on the North American Central High Plains. Aeolian Res. 10 (1), 53–59.
Vodonos, A., Friger, M., Katra, I., Avnon, L., Krasnov, H., Koutrakis, P., Schwartz, J., Lior, O., Novack, V., 2014. The impact of desert dust exposure on hospitalization due to the exacerbation of chronic obstructive pulmonary disease. Air Qual. Atmos. Health 7 (4), 433–439. http://dx.doi.org/10.1007/s11869-014-0253-z.
Yitshak-Sade, M., Novack, V., Katra, I., Gorodischer, R., Tal, A., Novack, L., 2014. Non-anthropogenic dust exposure and asthma medications purchase in children. Eur. Respir. J. 45, 652–660. http://dx.doi.org/10.1183/09031936.00078614.
Zobeck, T., Popham, T., Skidmore, E., Lamb, J., Merrill, S., Lindstrom, M., Mokma, D., Yoder, R., 2013. Aggregate-mean diameter and wind-erodible soil predictions using dry aggregate-size distributions. Soil Sci. Soc. Am. J. 67 (2), 425–436.